Analyst

Accepted Manuscript

ROYAL SOCIETY OF CHEMISTRY

www.rsc.org/analyst

Journal Name

RSCPublishing

ARTICLE

Monolayer Detection of Ion Binding at a Crown Ether-functionalised Supramolecular Surface *via* an Integrated Optical Bragg Grating

Richard M. Parker,[a,b] Dominic J. Wales,[a,b] James C. Gates,[b] Jeremy G. Frey,[a] Peter G. R. Smith[b] and Martin C. Grossel*[a]

Cite this: DOI: 10.1039/x0xx00000x

Received 00th January 2012,
Accepted 00th January 2012

DOI: 10.1039/x0xx00000x

www.rsc.org/

There have been significant recent developments in the field of integrated optical Bragg grating sensors for use in the biological domain, where changes in the thickness of a surface layer upon specific binding of biological targets allows quantitative detection. However in the chemical domain less work has been reported. We present here an integrated optical Bragg grating sensor, capable of evanescently detecting small changes in refractive index down to 10^{-6} RIU at infrared wavelengths, within a microfluidic system. The high spectral fidelity of the Bragg gratings combined with precise thermal compensation enables direct monitoring of the surface throughout the experiment. This allows the sensor to probe surface changes *in situ* and in real-time, from preparation through to chemical modification of the surface, so that the progress of dynamic surface-localized interactions can be followed. Here we describe confirmatory studies to validate this approach, including a comparison with the modelled optical system, before assessing the ability to detect binding of Group I cations at a crown ether-functionalised supramolecular surface. Unlike larger biological entities, for these small chemical species, simple additive changes in film-thickness no longer prevail.

Introduction

There have been significant developments in the field of optical refractometers for use in label-free detection within the biological domain.[1] Such refractometers have demonstrated high sensitivity to the change in thickness of a surface layer upon specific binding of biological targets.[2,3] One such refractometer is based on the use of Bragg gratings, optical components that act as a wavelength-selective reflectors, with the Bragg wavelength (λ_B) dependent on the near-field refractive index. Examples of Bragg grating biosensors include the detection of the hybridisation of DNA,[4] attachment of antibodies[5] and detection of biotoxins[6]. Historically Bragg gratings have been fabricated in optical fibre, offering inexpensive fabrication with easy and efficient signal delivery. However, one of the more recent advances is the use of Bragg grating sensors in planar silica waveguides to provide in-line optical sensing.[7,8] Such devices retain the advantages of optical fibre but offer enhanced functionality, including compatibility with microfluidics and the ability to multiplex sensor elements within a single device.

Although planar Bragg grating sensors have been successfully demonstrated in the field of label-free biological detection, little application towards the chemical domain has been demonstrated to date. One approach towards refractive index-based chemical detection is to exploit changes in the optical absorption of a thick film, as demonstrated by Girschikofsky,[9] where successful detection of naphthalene vapour down to 0.48 ppm was achieved using a dip-coated γ-cyclodextrin layer. However, this approach is inhibited by the need for the interrogation wavelength of the Bragg grating to be spectrally near to the absorption peak of interest. Alternatively the swelling of a polymeric hydrogel[10] layer can alter the measured refractive index *via* a change in the applied stress to the Bragg grating. Unfortunately, such thick-film approaches typically suffer from cross-sensitivity to competing analytes or limited porosity and slower diffusion within the active sensing layer.

Evolving from the biological analogue,[4] an active surface layer can be used to introduce the binding of specific chemicals at the surface. However, the order of magnitude smaller scale of chemical analytes prevents the thickness change upon surface binding from dominating the near-field sensing region. Within this regime not only must the explicit refractive index change of binding be considered, but also the influence of binding upon the monolayer environment. To ensure consistency between

sensors, the reproducibility of such a receptor layer is crucial and is dictated by the distribution and uniformity of the receptor surface and the thickness of this layer. By ensuring that only a discrete receptor monolayer is deposited on to the sensor surface, this thickness can be reproducibly controlled.

Surface-based chemistry has been utilised throughout nanoscience for assembling layers of molecules onto a substrate, often through the use of a self-assembled monolayer of a thiol or silane onto a gold or silica surface respectively. Many examples of chemically-modified silica surfaces have been demonstrated using organosilane chemistry, with (3-aminopropyl)triethoxysilane (3-APTES) commonly used in such systems to aminate the surface, allowing for the subsequent introduction of a wide range of functional moieties *via* peptide coupling.[11] Appropriate choice of head group allows for the properties of the surface to be controlled, from relative hydrophobicity or charge to potential receptor interactions.[12,13]

We have previously reported the detection of a nanometre-scale layer of amorphous silica *in vacuo* by a Bragg grating refractometer.[14] This demonstrated that the ability to detect a thin film of both comparable thickness and refractive index to a functional organic monolayer was within the sensitivity limit of the refractometer, however to date this has not been validated. Here we demonstrate a temperature-compensated integrated optical Bragg grating sensor incorporated within a microfluidic system, capable of precise refractive index measurements within a wide range of solvent systems. The ability to functionalize the planar surface of the microfluidic channel *in situ* with a self-assembled, functional organic monolayer is investigated in real-time and validated against the modelled optical system. With ions representing the smallest class of chemical analyte, investigating the ability to detect ion binding at the surface will probe the viability of the refractometer within a regime where, in contrast to bio-sensing, simple additive changes in film thickness no longer dominate. The ability of the integrated optical Bragg grating sensor to track changes in surface-localised refractive index is applied here to the investigation of the selectivity of a crown ether-modified supramolecular surface towards Group I salts.

Materials and Methods

An integrated optical waveguide circuit containing a series of four Bragg gratings was fabricated by direct UV-writing into the 6 μm thick photosensitive core layer of a planar glass structure, on a silicon substrate.[15,16] By altering the period of the Bragg grating, it was possible to 'write' multiple gratings over a wide wavelength range within a single waveguide channel. Each Bragg grating reflected a characteristic Bragg peak at a wavelength dependent on its local refractive index and grating period, as given by the Bragg condition. The Bragg wavelength can be determined from the reflectance spectrum, which in this work focuses upon the telecommunication wavelengths 1530-1570 nm (Figure S5, ESI). This was interrogated to sub-picometre resolution *via* optical fibre by an Exfo IQ-2300 erbium fibre-based amplified spontaneous emission (ASE) source with the reflected signal collected by an Ando AQ 6317B optical spectrum analyser (OSA), controlled *via* a PC running LabVIEW (Figure S4, ESI). For the silica-based devices reported here, robust alignment of a commercial optical fibre "pigtail" is routinely achieved through the use of commercial fibre v-groove technology, with less than 0.2 dB insertion loss. This device is all optical, requiring optical power below 1 mW, offering intrinsically safe operation in explosive vapour environments.

The Bragg gratings used here are inherently sensitive to temperature and strain, with a change of 1 ºC corresponding to a shift of only ~10 pm.[17] With removal of the cladding layer the evanescent field of the optical mode within the grating is exposed, allowing changes in the refractive index of the environment to alter the effective refractive index, n_{eff} of the Bragg grating; with the corresponding shift in the peak Bragg wavelength used to spectrally detect these changes. Sputtering a thin film of the high-index material, tantalum pentoxide, onto the sensor surface combined with precise monitoring of the Bragg wavelength of the grating allows for changes in the refractive index of the analyte to be monitored to 10^{-6} RIU.[14] By referencing against a second Bragg grating written adjacent to the etched region, it has been shown that the Bragg response due to changes in analyte refractive index can be separated from thermal and other effects using a simple first order approximation.[14]

The spectral nature of the measurement allows for a high dynamic range with Bragg wavelength shifts of ~10 nm achievable, corresponding to bulk refractive index changes in the analyte measurable from 1.00 to ~1.45. While the absolute sensitivity reported here is comparable to the state-of-the-art for other types of integrated refractometers employed in chemical sensing,[18] such as those based on surface plasmon resonance (SPR), the avoidance of bulk optics through the use of an optical fibre interconnect and the ability to self-reference *in situ* against physical effects is a significant advantage. Further, the ability to measure the absolute refractive index allows for continued measurement during significant changes in experimental conditions (e.g. changes in solvent) or between experiments which is extremely challenging with 'fringe counting' based approaches, as used in interferometric systems.

As we have previously reported,[19] such an integrated optical sensor can be readily incorporated within a microfluidic system to allow for *in situ* monitoring of a fluid flow. The reported microfluidic system was fabricated entirely from perfluorinated components and stainless steel and the same design is applied in this work (Figure S7, ESI). These robust materials allow for the use of harsh solvents and reagents that are typically incompatible with common polydimethylsiloxane (PDMS) based microfluidic systems, including strong acids and bases.[19]

An 18 μm deep trench was etched into the silica above three of the Bragg gratings, mechanically polished and sputtered with tantalum pentoxide, exposing the evanescent mode of the waveguide to the environment. The fourth Bragg grating was left unetched, allowing for referencing against physical phenomena. The etched trench was encapsulated within a

stainless steel flow cell fitted with a Kalrez™ O-ring to form a microfluidic channel. This flow cell was networked in series with a manifold solenoid valve that allowed for the controlled flow from up to six reservoirs, pushed through the system by a solenoid diaphragm pump. The pump rate and choice of reservoir was automated through a custom LabVIEW program *via* a USB DAQ controller. These components were linked *via* 400 µm bore ethylene tetrafluoroethylene (ETFE) tubing.

Results and Discussion

Formation and detection of a self-assembled monolayer

(3-Aminopropyl)triethoxysilane (3-APTES) is commonly used to form an amine-terminated self-assembled monolayer (SAM) on silica or silicone-based surfaces.[11] The quality of the silane layer formed is highly sensitive to the degree of free hydroxyl groups at the surface (e.g. patchy coverage), the presence of water (e.g. oligomerisation) and the nature of the leaving groups present. Accordingly, preparation of a silane monolayer can be subdivided into two distinct stages: cleaning and activation of the surface, followed by surface functionalisation. The deposition of a SAM can be readily realised within a microfluidic system, where the reagents can be flowed through the channels sequentially to any cleaning and/or preparative steps. This crucially allows for functionalisation of the surface *in situ* before recontamination can occur. The integrated optical Bragg grating refractometer additionally allows for real-time monitoring of the surface preparation steps and detection of the surface functionalisation process.

An etched sensor was fabricated with an overlayer of tantalum pentoxide (47 nm) and incorporated into the microfluidic flow system. Tantalum pentoxide was selected over other high-index materials (e.g. titanium dioxide) due to both its ease of deposition and the presence of a hydroxyl surface allowing it to be chemically-functionalised analogously to silica.[20] The sensor surface was cleaned by an automated series of washes with water and acetone, followed by 5.0 M potassium hydroxide to restore the hydroxyl surface. To deposit the SAM, a 10 % *v/v* solution of 3-APTES in distilled ethanol was flowed over the freshly cleaned surface. This was followed by fluorescein isothiocyanate (FITC, 20 mg in 150 mL dimethylsulphoxide), allowing independent detection of the SAM by fluorescence microscopy. After cleaning, and between each subsequent functionalization of the surface, the shift in Bragg wavelength was recorded for a flow of an ethanol reference solution. With temperature suitably compensated, any change in refractive index observed should arise from displacement of ethanol at the surface with the higher index monolayer. Figure 1 illustrates the real-time average Bragg grating response during surface preparation and immediate functionalisation with 3-APTES, within the microfluidic flow reactor, with the inset focusing on the 7 pm direct increase in Bragg wavelength during SAM formation. It was observed that after functionalisation with 3-APTES an average increase in Bragg wavelength of 6 (±2) pm (Δn_{eff} = 5.6 x 10^{-6} RIU) was observed in the ethanol reference, which increased to 56 (±4) pm (5.3 x 10^{-5} RIU) with the subsequent attachment of FITC.

It should be noted that upon switching between solutions, non-instantaneous changes in refractive index were observed. These were particularly apparent upon switching between ethanol-water or acetone-water, where 'spikes' in refractive index were observed. As we have previously reported these slow transients are not surface effects, but the result of solvent dispersion within the microfluidic channel, with the 'spikes' caused by a non-linear refractive index mixing profile.[19]

Attachment of 3-APTES to a silica surface was independently confirmed by contact angle goniometry of a 1.0 µL water droplet. A deactivated silica surface was found to

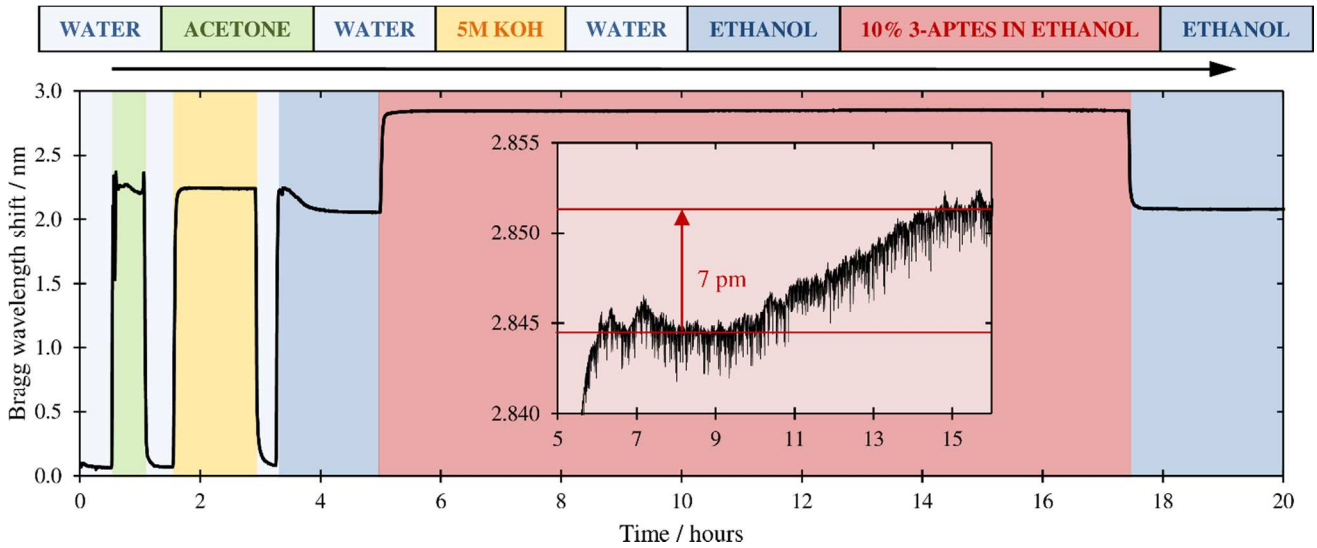

Fig. 1 The average Bragg wavelength shift for the three sensor Bragg gratings during surface preparation with: water, acetone and 5.0 M aqueous potassium hydroxide and subsequent functionalisation of the surface with 3-APTES, as a continuous and automated process within the microfluidic flow reactor. Thermal drift was compensated by referencing against a fourth, unetched Bragg grating. The inset graph shows the 7 (±2) pm increase in Bragg wavelength during exposure to 10% *v/v* 3-APTES in ethanol. After attachment a shift of +6 (±2) pm was measured in ethanol, relative to the initial ethanol reference.

have a contact angle of ~ 35 °, corresponding to a mildly hydrophobic surface. On cleaning, the contact angle reduced to below the limit of the goniometer (<5°) indicating a hydrophilic surface. Upon functionalisation with 3-APTES, the contact angle increased to 53 (±4)°, consistent with literature.[21] The presence of the FITC-APTES monolayer on the surface was confirmed by fluorescence microscopy (Ex: 467-498 nm, Em: 513-556 nm).

Surface contamination in air was observed, with the hydrophobicity of an activated tantalum pentoxide surface seen to increase over the course of several minutes outside of the microfluidic device. This demonstrated the need to functionalise the surface immediately after cleaning; however, once treated with 3-APTES the surface was found to be more resilient, with consistent contact angle measurements being observed over several days.

Modelling of the self-assembled monolayer

In order to validate that the system is capable of reliable analytical operation with a functional monolayer it was important to confirm that the device and protocol were robust to factors such as system cleanliness, film thickness and the surface roughness of the sensor. The intensity distribution of the optical mode within the FITC-APTES SAM sensor system was modelled using the commercial waveguide mode solving software, *Fimmwave*. The modelled waveguide was calibrated against the sensitivity of the etched sensor to a series of Cargille refractive index liquids (Series AA and AAA), both before and after deposition of tantalum pentoxide (Figure 2a). This allowed for factors such as the etch depth, the refractive index step of the waveguide core and the tantalum pentoxide thickness to be corroborated (see Figure S8 and the ESI for further discussion of this approach and the modelled parameters). This model was then used to predict the effect of depositing a film of refractive index, n of 1.44 (comparable to that of a 3-APTES monolayer) and a film of 1.74 (comparable to that of the FITC-APTES monolayer) onto the sensor surface, with an effectively infinite layer of ethanol above (n = 1.35).

The model predicted that for the deposition of a very thin film of refractive index 1.44 on the sensor surface, a linear shift in peak Bragg wavelength of 10 pm for each nanometre deposited would be observed (Figure 2b). A monolayer of 3-APTES is approximately 0.7 nm thick[22] and therefore should produce a shift of 7 pm. This predicted shift is consistent within error with the experimental value of 6 (±2) pm, allowing for the assumption in the model that an amorphous layer of 3-APTES was deposited on the surface rather than a discrete molecular film with a limited packing density. As a result of the higher refractive index of the fluorescein dye, the modelled effective index change of the waveguide as a function of film thickness showed an increase in sensitivity, with a predicted shift in peak Bragg wavelength of 51 pm per nanometre deposited onto the surface, for small values of film thickness (Figure 2c). A monolayer of FITC-APTES is approximately 1.2 nm thick[22] and therefore should result in a shift of 60 pm, again consistent with the experimental value of 56 (±4) pm.

Due to the nano-scale thickness of the self-assembled monolayer, variations in surface roughness are expected to have a significant impact on the surface area of the film and ultimately the sensitivity and reproducibility of the system. The assumption of a smooth surface represents the most significant assumption in the model and as such, atomic force microscopy was employed to investigate the surface roughness of the polished channel. The roughness of the polished sensor surface was found to be comparable to that of the unetched surface, with a 2-D arithmetic roughness, R_a < 0.8 nm, and as such is expected to have little effect once averaged over the length of the 2.0 mm Bragg grating.

There is good agreement between the modelled and experimental refractive index shift upon attachment of the small organic molecule, FITC, to the 3-APTES SAM surface. This confirms that modelling the reaction as the displacement of a thin solvent layer is applicable when little change in the

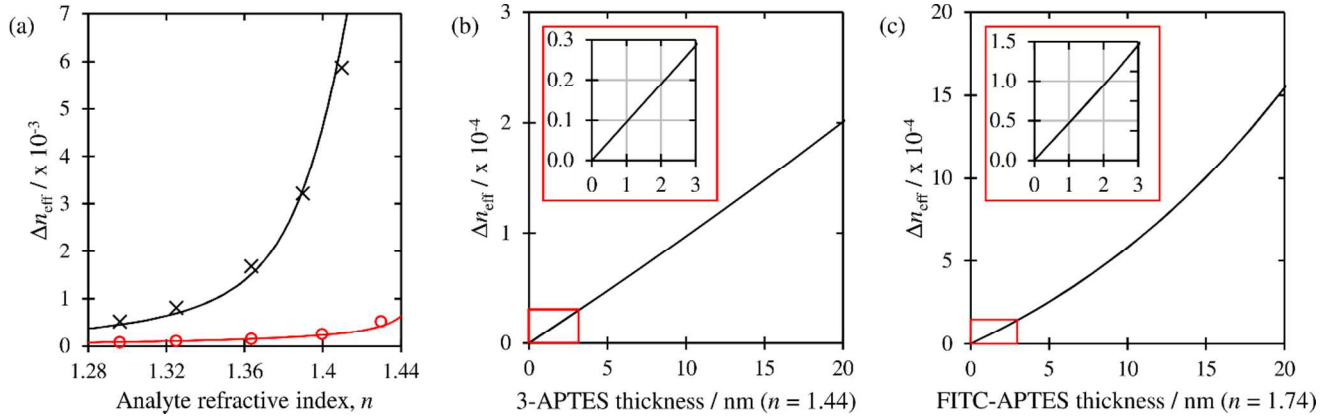

Fig. 2(a) A comparison of the modelled (line) and experimental (marker) effective refractive index of the optical mode of the waveguide for increasing analyte refractive index for both the bare (**o**) and tantalum pentoxide coated (**x**) sensor. **(b)** The modelled change in effective refractive index on increasing the thickness of a thin film of refractive index 1.44, comparable to 3-APTES and **(c)** a film of refractive index 1.74, comparable to FITC-APTES monolayer. The insets display the linear relationship observed over monolayer-scale film thicknesses and correspond to the regions at the origin marked in red in **(b)** and **(c)**, with the axis scale unchanged.

interaction with the solvent at the surface is anticipated and a measurable change in monolayer thickness occurs. For smaller reactants (e.g. ions) manipulation of the refractive index of the monolayer itself is expected to dominate.

Validation of the self-assembled monolayer

To confirm that the deposited layer was discrete rather than oligomeric, the Bragg wavelength shift was compared with that of the analogue (3-aminopropyl)dimethylethoxysilane (3-APDMS). 3-APDMS contains only a single *ethoxy*- ligand inherently restricting deposition to a single monolayer and has a refractive index comparable to 3-APTES;[23] if 3-APTES is forming a discrete monolayer under the conditions used here the Bragg response upon SAM deposition should be comparable. To amplify any differences in the refractive index from surface functionalization with these two reagents, a second device was fabricated with a thicker tantalum pentoxide overlayer (50 nm) that was twice as sensitive to changes in refractive index, at the expense of dynamic range. Deposition of 3-APTES onto this new device was found to give a Bragg wavelength shift of 14 (±1) pm, while the same experiment with 3-APDMS resulted in a Bragg wavelength shift of 11 (±3) pm. Allowing for subtle differences in refractive index between 3-APTES and 3-APDMS, the surface topography and the uncertainty of the Bragg sensitivity of the sensor gratings, these shifts are consistent. It should be noted that the ability of 3-APDMS to only form a single bond with the surface results in a much more labile monolayer than with 3-APTES.[24]

This successful comparison between the deposited layer and a known monolayer, in addition to the consistency with the modelled planar sensor system, confirms that this protocol allows for the production of a molecular monolayer on the surface. With successful detection of the covalent attachment of a small organic molecule to the monolayer by surface-localised refractive index, the refractometer was then employed towards detecting cation binding at the surface, where the small size and charge of such species is anticipated to have an effect on the nature of the refractive index shift observed.

Investigation into selective and reversible ion binding at a supramolecular-functionalised surface

Crown ethers are macrocyclic molecules that consist of a ring of ether groups and as such represent one of the simplest host-guest systems in supramolecular chemistry.[25] The size of the cavity within the macrocycle strongly determines which cation will bind most favourably, with Nakajima reporting that crown ethers immobilized on a silica surface have sufficient selectivity to chromatographically separate mixed salts.[26] The crown ether, benzo-15-crown-5, is known to exhibit size-selectivity for sodium over other Group I metal cations.[27] To allow attachment to the 3-APTES SAM, the derivative 4'-(chlorocarbonyl)benzo-15-crown-5 (**3**) was synthesized in three steps, as shown in Figure 3a (synthesis and characterisation is included in the ESI).

A sensor sputtered with 72.5 nm of tantalum pentoxide was fabricated, before encapsulating it within the microfluidic flow cell. The high sensitivity of this sensor afforded by the thicker tantalum pentoxide layer reduced the dynamic refractive index range to 1.00 – 1.35 with acetone representing the upper limit of a compatible solvent (Figure S6, ESI). To allow for

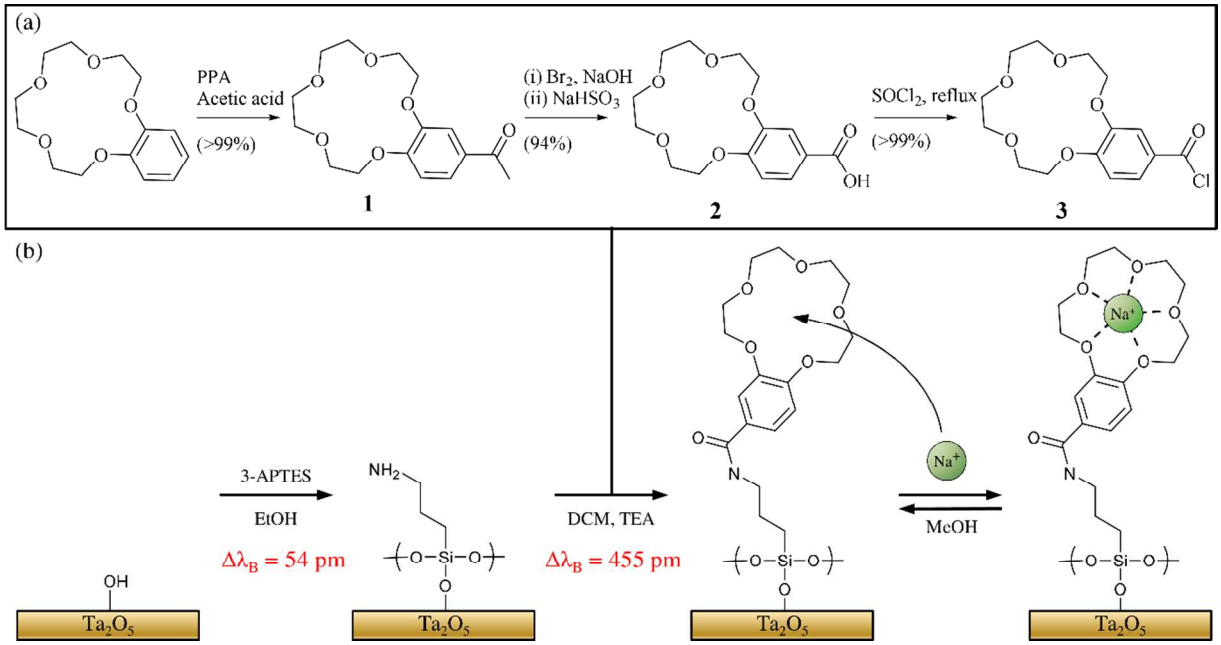

Fig. 3(a) Synthesis of 4'-(chlorocarbonyl)benzo-15-crown-5 (**3**) from benzo-15-crown-5 in 3 steps, with high yield. **(b)** Schematic illustrating the step-wise formation of the sensor surface within the microfluidic channel; after cleaning and preparative steps the sensor surface is first treated with 3-APTES to form an amine-terminated SAM, followed by **3** to introduce the crown ether moiety. The Bragg wavelength shift on addition of each component was recorded against a methanol reference. As shown schematically, the crown ether monolayer will reversibly bind a sodium cation within the macrocyclic cavity.

continued and consistent monitoring throughout SAM deposition, modification and surface binding processes, a switch from ethanol to the lower refractive index solvent, methanol was necessary (n = 1.33). It was observed that the Bragg response to methanol after surface functionalisation with 3-APTES was shifted by 54 (±4) pm to higher wavelength comparable to the 38 (±4) pm increase in Bragg wavelength over the period of the 3-APTES/methanol wash. After subsequent attachment of the crown ether, **3**, a further increase by 455 (±5) pm was observed in methanol (see Figure S2). A control was conducted where the procedure to attach **3** onto a sensor was repeated in the absence of a 3-APTES monolayer, this resulted in no observed increase in Bragg wavelength. This is used as evidence that this increase in Bragg wavelength is exclusively the result of **3** bonding to the 3-APTES monolayer surface. Similarly flowing only solvents over the 3-APTES surface did not give rise to a permanent Bragg wavelength shift. While these shifts are an order magnitude larger than for the modelled sensor, this is due to the greater Bragg response to refractive index change the thicker tantalum pentoxide layer affords (Figure S6, ESI). Interestingly, both the attachment of FITC and **3** were observed to give a ~9x greater Bragg wavelength shift that that recorded for the deposition of the respective 3-APTES monolayer.

As illustrated schematically in Figure 3b, a sodium cation can bind within the macrocyclic crown ether at the surface, however this association is in equilibrium with the bulk media, allowing the surface to be restored by washing with pure methanol. The crown ether-functionalized surface was exposed to a 10 mM flow of sodium chloride in HPLC methanol. The temporal Bragg wavelength shift upon is shown in Figure 4, where it was found that it took up to an hour for the surface to fully equilibrate with no further changes in Bragg wavelength upon exposure to the flowing salt solution. Upon switching back to a flow of pure methanol, this trend in the Bragg wavelength was reversed over a comparable time-scale and is attributed to the restoration of the sensor surface.

This crown ether-functionalized surface was exposed to a series of Group I metal halides in decreasing concentration from 10 mM down to 1.0 µM in HPLC methanol. As shown in Figure 5, the Bragg wavelength shifts recorded for the sensor followed the trend expected for benzo-15-crown-5,[27] with the magnitude of the wavelength shift upon binding to sodium more than three times that seen for other Group I cations. Weaker binding at the surface was still observed for other cations, where the size mismatch between the cations and the flexible macrocyclic cavity is not so great as to prevent a weak association.[28] While potassium can form a 2:1 sandwich complex with benzo-15-crown-5 that rivals the binding of sodium,[29,30] the minimal enhancement of potassium over lithium implies that the geometry of the surface is too confined for such sandwich complexes to readily occur.

In stark contrast to the attachment of the small organic molecule (FITC) and counter to the thick-film biological regime, the Bragg wavelength shift upon binding was observed to result in a decrease in Bragg wavelength and therefore a reduction in refractive index. This is contrary to the effect observed in bulk sensing of salt solutions, where a positive

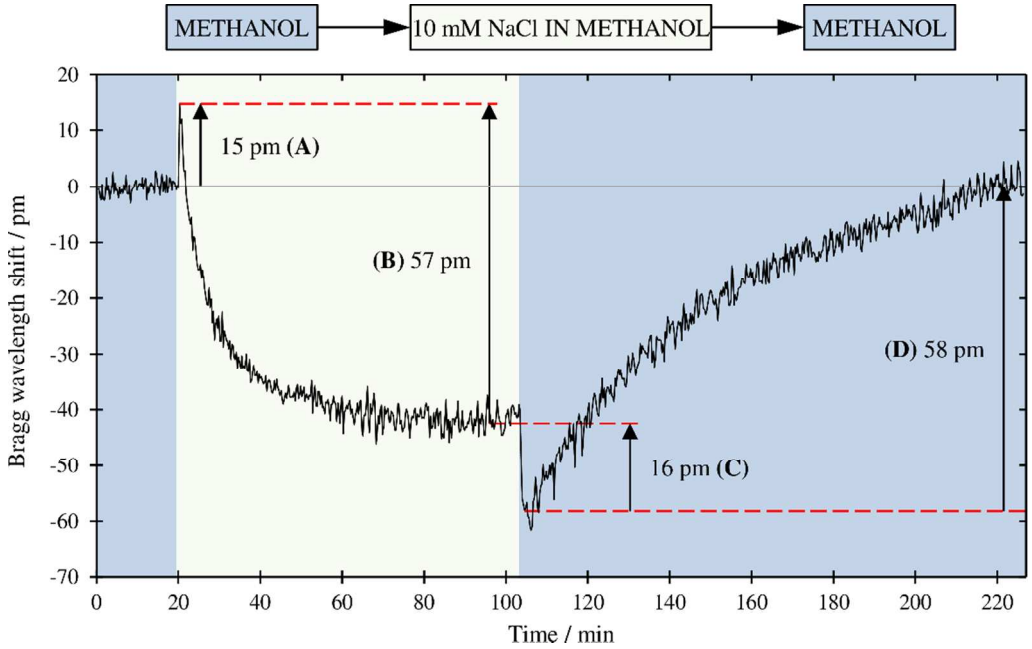

Fig. 4 The average Bragg wavelength shift over time for the crown ether functionalised sensor as the microfluidic flow is alternated between HPLC methanol and a solution of 10 mM sodium chloride in methanol. Upon switching to the salt solution (t = 20 min) an initial sharp increase of 15 (±2) pm was observed (A), followed by a gradual decrease in Brag wavelength of 57 (±2) pm over the following hour (B). Upon returning the microfluidic flow to pure methanol this trend was reversed, with a rapid drop of 16 (±2) pm (C) followed by a gradual increase of 58 (±2) pm to the initial value over a comparable timescale (D). This trend is attributed to the reversible binding of sodium within the crown ether macrocycle.

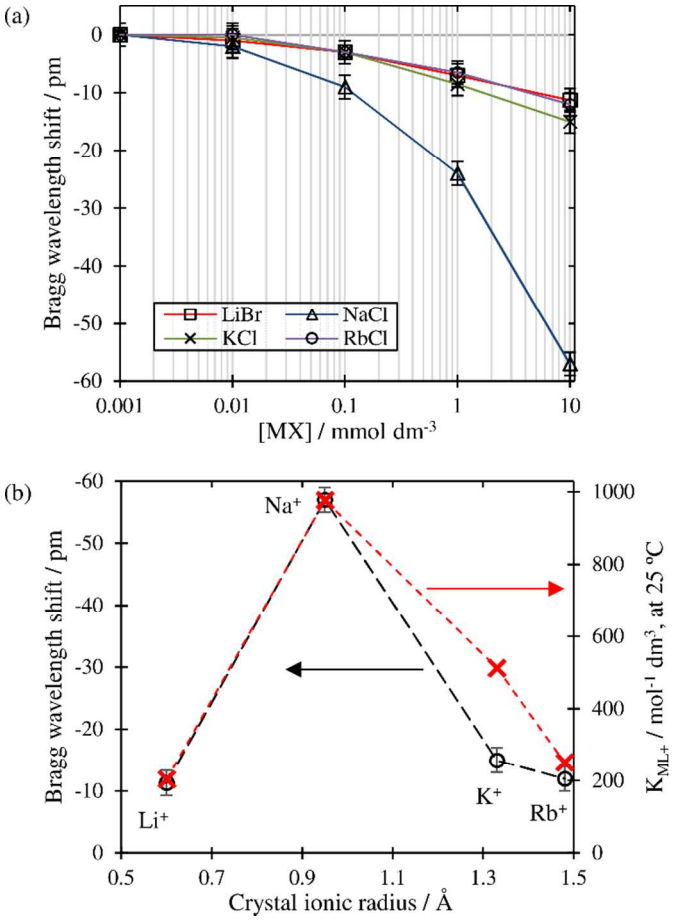

Fig. 5(a) The Bragg wavelength shift of the crown ether monolayer sensor as a function concentration for lithium, sodium, potassium and rubidium salts in methanol, plotted on a logarithmic *x*-axis. Error bars represent the peak deviation between measurements of ±2 pm. **(b)** Comparison of the Bragg wavelength shift of the crown ether monolayer on exposure to a series of 10.0 mM Group I alkali salt solutions (**o**) with the corresponding reported formation constant, K_{ML} for complexes of benzo-15-crown-5 in methanol (**x**),[27] as a function of ionic radius. The discrepancy observed for potassium is attributed to geometric confinement of benzo-15-crown-5 at the surface.

index shift is measured for increasing salt concentration. Examining the raw data for the 10 mM solutions for both the bare and functionalized systems (Figure 6), it was observed that there are two components, a fast initial positive shift, that is equal in magnitude for both surfaces, which is then followed by a slow decrease in Bragg wavelength for the functionalized surface. The first rapid increase is attributed to the bulk refractive index of the analyte solution, while the second represents the gradual binding of sodium to the surface. This temporal refractive index profile is similarly observed in Figure 4, where the rapid increase upon switching to 10 mM sodium chloride (A) is matched in magnitude by the rapid decrease upon reverting to a methanol flow (C). For more dilute solutions the increase due to the bulk solution is below the sensitivity threshold and only the slow decrease is observed, whilst for significantly higher concentrations the sharp bulk transition becomes dominant. This effect could be applied in future through the use of an etched, but unfunctionalised reference grating, allowing decoupling of any fluctuations in the refractive index of the analyte solution from that at the surface.

In the case of the benzo-15-crown-5 SAM surface layer, it is expected that diffusion of cations into the layer is occurring. It is postulated that this diffusion and subsequent binding of cations into the benzo-15-crown-5 SAM layer, results in a change in the density and consequently the effective index of the monolayer. It is known that upon binding of a cation in a crown ether that there is a significant change in the solvation of the crown ether motif.[31] In addition, it is known that a cation within a crown ether's cavity can still be solvated with solvent molecules together with an associated solvated counter anion.[32] It is proposed that these associated solvent molecules and counter anion increase the steric bulk of the crown ether-cation complexes relative to the uncomplexed crown ether and thus decrease the density of the monolayer; the presence of the lower refractive index solvent molecules in the free volume lowers the effective index of the crown ether monolayer. In addition, upon formation of the overall positively charged cation-crown ether complex, there would be electrostatic repulsion between adjacent cation-crown ether complexes. This would further decrease the density of the monolayer, the free volume being filled with lower refractive index solvent molecules. Therefore, it is postulated that the reordering of the structure of the solvation environment of the benzo-15-crown-5 SAM contributes to the observed reduction in refractive index.

With the crown ether motif known to demonstrate a moderate degree of selectivity over other Group I metals and given the trend observed in Figure 5a, an investigation into a mixed analyte systems was briefly explored. A mixed solution of 10 mM sodium chloride and 10 mM potassium chloride was flowed over the sensor surface and compared to that of the corresponding individual solutions. It was observed that the resultant Bragg wavelength shift for the mixed solution was 73 (±3) pm, greater than that of a 10 mM sodium chloride solution alone. As saturation of the crown ether monolayer was not observed with 10 mM [NaCl], and weak binding to potassium has been shown to occur, it is likely that both sodium and potassium are simultaneously binding to the surface, with the resultant Bragg wavelength shift representing this cumulated effect. Indeed the combined shift for individual sodium and potassium solutions was consistent, within error, with the mixed solution. This demonstrates the need for the suppression of undesired binding to achieve selectivity in a chemical sensor.

Performance, reliability and reproducibility of the optical sensor

While the performance of this sensor with respect to absolute sensitivity to sodium concentration is not competitive with the state-of-the-art reported within the broader sensor community, much of the limitations in terms of sensitivity and selectivity are attributed to the use of crown ether as the active sensing element. Benzo-15-crown-5 was specifically employed here as it represents a well-studied and robust interaction

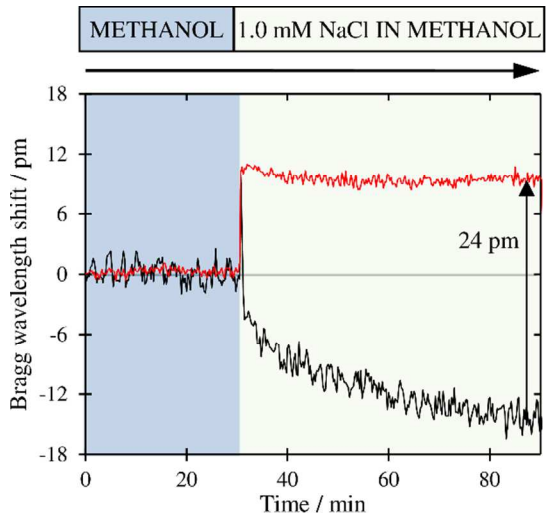

Fig. 6 Comparison of the Bragg response upon switching from methanol to a 1.0 mM sodium chloride solution for the bare (red) and crown ether functionalized (black) sensor surfaces.

allowing for the efficacy of the sensor to monolayer-scale changes, rather than the binding interaction, to be investigated. It is believed that the use of an infrared chromoionophore with more pronounced size exclusion properties (e.g. a modified calix[4]crown)[33] would improve the performance of the device. Similarly, the slow equilibration time for the active monolayer (up to 1 hour) is impractical for real-world applications, however this is attributed to laminar flow within the microfluidic analysis channel and could be shortened by inducing turbulence in the micro-channel. However, it should be noted that the optical sensor itself, when compared to other integrated optical sensors,[18] is competitive in terms of both the dynamic range and sensitivity to changes in surface-localised refractive index. While interferrometric techniques (e.g. Mach-Zehnder) can in principal offer higher sensitivity (up to 10^{-8} RIU)[18], the difficulties in referencing physical phenomena and responding to rapid large changes in refractive index (e.g. switching solvents) in combination with the inability to multiplex into distributed networks inhibit their real-world deployment.

While only a single device was used for each component of the experiments; for the data collected in Figure 5a this represents 160 h of continuous operation without loss of performance. Further, the fabrication of the optical sensor is highly reproducible, with deposition of the refractive index and thickness of the planar glass layers by flame hydrolysis deposition and the UV-writing of waveguides highly automated. The wet etching of the microchannel is undertaken using real-time feedback from the Bragg gratings, which in combination with precise deposition of a high-index overlayer of known refractive index allows for near-identical sensitivity between multiple gratings within a device. Finally the ability to calibrate the sensor during each step of the fabrication process allows for both the ability to scale data between sensors with different geometries (Figure S6, ESI) and for accurate modelling of the optical properties of the waveguide.

Conclusions

The use of a high fidelity Bragg grating sensor has been demonstrated to be able to probe reactions at a surface through monitoring changes in refractive index. The attachment of a monolayer of 3-APTES was detected and its discrete nature corroborated by comparing the change in refractive index recorded with that of the modelled optical system and that of the analogue, 3-APDMS.

The Bragg grating refractometer successfully probed the binding of a benzo-15-crown-5 monolayer down to sodium chloride concentrations of 10 µM in methanol. The trend across Group I salts followed that predicted by the formation constant,[27] with a much greater refractive index change upon coordinating sodium, allowing for differentiation from competing salts at 100 µM concentrations. The weak refractive index response with potassium is attributed to geometric confinement of the complex to the surface. The reduction in the surface-localised refractive index upon binding ions to the surface was unexpected and is in stark contrast with the biological regime. It is hypothesised that the attachment of a monolayer of a small organic molecule (e.g. FITC) can be considered as the displacement of solvent with a thin-film of amorphous material, analogously to the thick-film biological regime. However when coordination of the ionic guest involves ingress into the host, resulting in a change of shape and solvation of the entire layer, binding cannot be simply considered an additive process, but rather the induced effect of binding upon the refractive index of the monolayer as a whole must be considered.

This ability to directly observe supramolecular complexation in real-time upon a planar surface *via* refractive index, will in future allow for the interrogation of more complex and dynamic supramolecular interactions, without the constraints of molecular labelling. While many other analytical techniques are limited to the use of mesoporous or thick films to achieve the required sensitivity, here we do not require this approach. However, the advantages gained through the use of a high surface area matrix are compatible with the integrated optical Bragg grating sensor and when appropriate, can lead to further enhancements in sensitivity.[34]

While UV-writing is ideal for rapid prototyping, it is envisaged that high-throughput production of such optical sensor could be achieved by photolithography, allowing he sensors to be produced relatively cheaply (<$1), with reconditioning of the sensing layer to increase their lifespan. The largest cost to the end user is the laser-based analytical system; however the option to spectrally address multiple sensors, multiplexed within a distributed network allows for a single analytical system to probe, for example, an entire manufacturing plant.

Notes and references

[a] School of Chemistry, University of Southampton, Highfield, Southampton, SO17 1BJ (United Kingdom). *E-mail: M.C.Grossel@soton.ac.uk

[b] Optoelectronics Research Centre, University of Southampton, Highfield, Southampton, SO17 1BJ (United Kingdom)

Electronic supplementary information (ESI) available: Synthetic methods and characterisation, integrated Bragg grating sensor fabrication, calibration and analysis protocols; with supporting figures.

1. X. Fan, I. M. White, S. I. Shopova, H. Zhu, J. D. Suter, and Y. Sun, *Anal. Chim. Acta*, 2008, **620**, 8–26.
2. A. V Dotsenko, A. L. Diikov, and T. A. Vartanyan, *Sensors Actuators B Chem.*, 2003, **94**, 116–121.
3. J. Homola, S. S. Yee, and G. Gauglitz, *Sensors Actuators B Chem.*, 1999, **54**, 3–15.
4. A. N. Chryssis, S. S. Saini, S. M. Lee, H. Yi, W. E. Bentley, and M. Dagenais, *IEEE J. Sel. Top. Quantum Electron.*, 2005, **11**, 864–872.
5. M. P. DeLisa, Z. Zhang, M. Shiloach, S. Pilevar, C. C. Davis, J. S. Sirkis, and W. E. Bentley, *Anal. Chem.*, 2000, **72**, 2895–2900.
6. D. Bhatta, E. Stadden, E. Hashem, I. J. G. Sparrow, and G. D. Emmerson, *Sensors Actuators B Chem.*, 2010, **149**, 233–238.
7. S. Watts, *Nat. Photonics*, 2010, **4**, 433–434.
8. I. J. G. Sparrow, P. G. R. Smith, G. D. Emmerson, S. P. Watts, and C. Riziotis, *J. Sensors*, 2009, **2009**, 607647.
9. M. Girschikofsky, M. Rosenberger, S. Belle, M. Brutschy, S. R. Waldvogel, and R. Hellmann, *Sensors*, 2012, **12**, 2018–2025.
10. J. Cong, X. Zhang, K. Chen, and J. Xu, *Sensors Actuators B Chem.*, 2002, **87**, 487–490.
11. C. Malins, S. Fanni, G. Glever, J. Vos, and B. D. MacCraith, *Anal. Commun.*, 1999, **36**, 3–4.
12. S. A. Kulkarni, S. B. Ogale, Kunjukrishana, and P. Vijayamohanan, *J. Colloid Interface Sci.*, 2008, **318**, 372–379.
13. C. Haensch, S. Hoeppener*, and U. S. Schubert, *Chem. Soc. Rev.*, 2010, **39**, 2323–2334.
14. R. M. Parker, J. C. Gates, M. C. Grossel, and P. G. R. Smith, *Appl. Phys. Lett.*, 2009, **95**, 173306.
15. M. Svalgaard and M. Kristensen, *Electron. Lett.*, 1997, **33**, 861–863.
16. G. D. Emmerson, S. P. Watts, C. B. E. Gawith, V. Albanis, M. Ibsen, R. B. Williams, and P. G. R. Smith, *Electron. Lett.*, 2002, **38**, 1531–1532.
17. R. M. Parker, J. C. Gates, M. C. Grossel, and P. G. R. Smith, *Sensors Actuators, B*, 2010, **145**, 428–432.
18. P. V Lambeck, *Meas. Sci. Technol.*, 2006, **17**, R93–R116.
19. R. M. Parker, J. C. Gates, D. J. Wales, P. G. R. Smith, and M. C. Grossel, *Lab Chip*, 2013, **13**, 377–385.
20. R. De Palma, W. Laureyn, F. Frederix, K. Bonroy, J.-J. Pireaux, G. Borghs, and G. Maes, *Langmuir*, 2007, **23**, 443–451.
21. D. G. Kurth and T. Bein, *Angew. Chem.*, 1992, **31**, 336–338.
22. P. Mela, S. Onclin, M. H. Goedbloed, S. Levi, M. F. Garcia-Parajo, N. F. van Hulst, B. J. Ravoo, D. N. Reinhouldt, and A. van den Berg, *Lab Chip*, 2005, **5**, 163–170.
23. S. S. Saini, C. Stanford, S. M. Lee, J. Park, P. DesShong, W. E. Bentley, and M. Dagenais, *IEEE Photonics Technol. Lett.*, 2007, **19**, 1341–1343.
24. C. Wittmann, *Top. Curr. Chem.*, 2005, 261.
25. C. J. Pedersen, *J. Am. Chem. Soc.*, 1967, **89**, 7017–7036.
26. M. Nakajima, K. Kimura, and T. Shono, *Anal. Chem.*, 1983, **55**, 463–467.
27. Y. Takeda and T. Kumazawa, *Bull. Chem. Soc. Japan*, 1988, **61**, 655–658.
28. E. Wagner-Czauderna, A. Koczorowska, and M. K. Kalinowski, *J. Coord. Chem.*, 1999, **46**, 265–276.
29. F. Arnaud-Neu, M.-J. Schwing-Weil, K. Ziat, S. Cremin, S. J. Harris, and M. A. McKervey, *New J. Chem.*, 1991, **15**, 33–37.
30. P. R. Mallinson and M. R. Truter, *J. Chem. Soc. Perkin Trans. 2*, 1972, 1818–1823.
31. A. Y. Friedzon, A. A. Bagatur'yants, S. P. Gromov, and M.V. Afimov, *Russ. Chem. B. Int. Ed.*, 2005, **54**, 2042–2054.
32. T. Okada and T. Usui, *J. Chem. Soc., Faraday Trans.*, 1996, **92**, 4977–4981.
33. T. Hayashita, K. Kunogl, H. Yamamoto, and S. Shinkai, *Anal. Sci.*, 1997, **13**, 161–166.
34. D. J. Wales, R. M. Parker, J. C. Gates, M. C. Grossel, and P. G. R. Smith, *Sensors Actuators B Chem.*, 2013, **188**, 857–866.

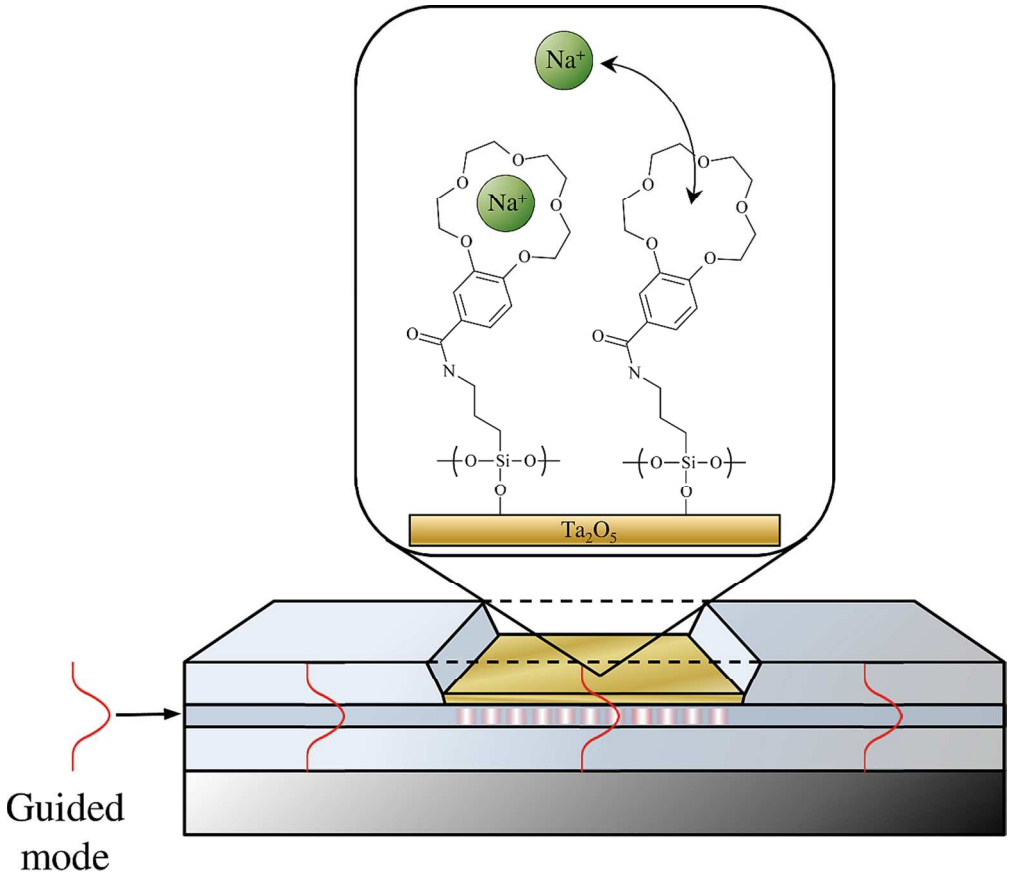

The formation, detection and validation of a self-assembled monolayer by an integrated optical Bragg grating is reported, allowing investigation into the surface-localised change in refractive index upon ion binding at a supramolecular monolayer."